

Prediction of Interfacial Cracking due to Differential Drying Shrinkage of Concrete in Precast Shell Pier Cap

Kyong Pil Jang¹, Je kuk Son² and Seung Hee Kwon^{1,3}

Abstract: In a precast shell pier cap, cracking at the interface between the precast shell and the cast-in-place concrete may happen due to differences between the drying shrinkage of the inner and the outer concrete. The objective of this study is to establish a prediction method for interfacial cracking that will consider the real mechanism of differential drying shrinkage and creep. The main parameters used in the analysis were determined from experiments for a concrete mix that is applied to the manufacturing of pier caps. The variation of internal relative humidity over time was first calculated based on the nonlinear moisture diffusion; cracking analysis then followed. Prediction of the initiation of interface cracks and the increase of their width over time was performed. It was found that additional reinforcement across the interface is very effective at reducing crack width.

Keywords: Interfacial cracking, Precast pier cap, Differential drying shrinkage, Creep, Moisture diffusion.

1 Introduction

In recent years, numerous efforts have been made to speed up the construction process of concrete bridges by assembling prefabricated structural segments. Rapid construction provides a lot of benefits in many aspects such as improvement in economy, reduction in traffic delay near the construction sites, and enhancement in working zone safety [Chung, Lee and Gil (2013); Park, Park and Cho (2013); Kim, Lee, Kim and Shin (2010); Lee, Son, Yoo and Shin (2010); Shim, Chung and Kim (2008)].

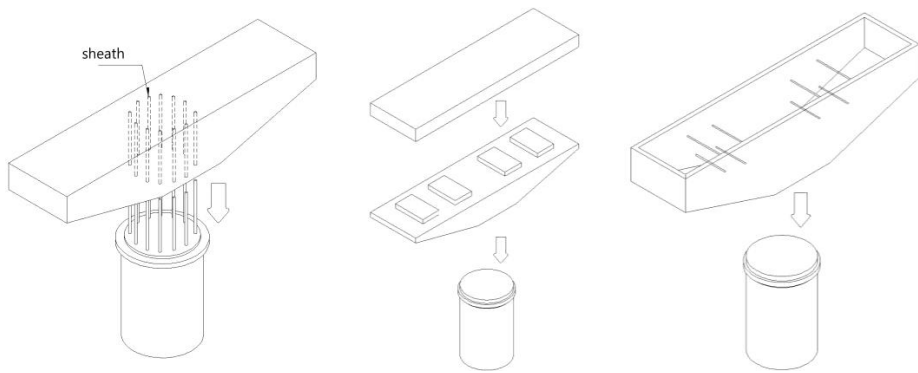
¹ Department of Civil and Environmental Engineering, Myongji University, San 38-2, Namdong, Cheoin-gu, Yongin, Gyeonggi-do, 449-728, South Korea.

² Construction Technology Research Institute, Samsung C&T Corporation, 6th Floor, Yeoksam-dong, Gangnam-gu, Seoul, 135-935, South Korea.

³ Corresponding author.

Tel.: +82 (31) 330-6418; Fax: +82 (31) 336-9705; E-mail: kwon08@mju.ac.kr

As for the pier cap in the substructure, several methods have also been suggested, as schematically illustrated in Fig. 1 [Lee, Son, Yoo and Shin (2010)]. The simplest method is one in which the whole part of pier cap is first manufactured with precast concrete; the pier cap is next hoisted and installed on the top of the pier by a heavy crane; finally, the pier and the pier cap are tightened through prestressing or continuous rebar. However, the weight of the whole pier cap is very heavy and difficult to efficiently handle, and so a crane and a vehicle of large capacity should be used in the construction.



(a) Full precast pier-cap (b) Segmented precast pier-cap (c) Precast shell pier-cap

Figure 1: Existing methods for fast construction of pier-cap

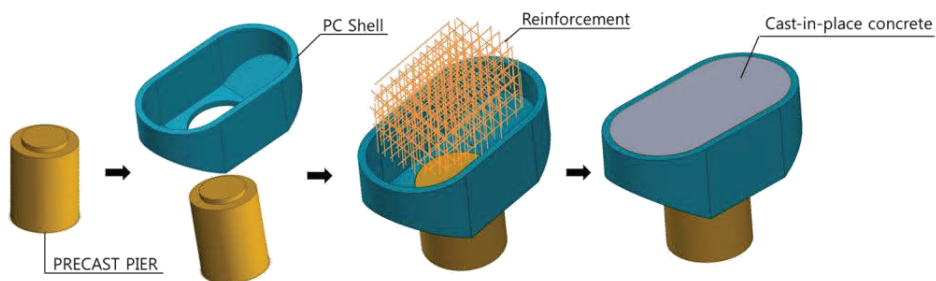


Figure 2: Construction process of precast shell pier-cap

Another method is to assemble prefabricated precast segments of the pier cap over the pier. This process also incurs some difficulty in handling the segments in the air and in ensuring the bonding at the interfaces between the segments.

One other method is to first fabricate the outer shell of the pier cap with precast concrete and then locate that over the top of the pier; next, the pre-assembled reinforcement cage is put into the shell; finally, concrete is poured into the shell at the site, as shown in Fig. 2. The outer shell is used as a permanent formwork as well as a part of the structural member. This method provides easy handling of the outer shell due to its lower weight; it is cost effective because construction equipment of smaller capacity can be used; and it is very beneficial especially for construction in downtown areas because the use of the smaller size equipment can minimize the number of the traffic lanes that must be closed in the middle of construction.

Several studies that have tried to investigate the structural safety of precast (PC) shell pier cap have been previously performed; these studies verified that the structural performance of a precast shell pier cap, in aspects such as strength and ductility, is almost equal to that of a conventional pier cap of the same size [Lee, Son, Yoo and Shin (2010)]. However, there is a problematic issue in terms of serviceability and durability of the PC shell pier cap, that is, potential cracking at the interface between the PC outer shell and the inner cast in-place concrete, as shown in Fig. 3. Interfacial cracking may be induced due to the difference between the drying shrinkages of the outer and the inner concrete. If the crack width does not meet the specifications for durability in the design code, usually 0.3 mm for general conditions, applications of PC shell pier caps to construction would be very limited. Therefore, a method is needed to predict cracking before construction and to establish countermeasures to prevent cracks larger than the specified crack width.

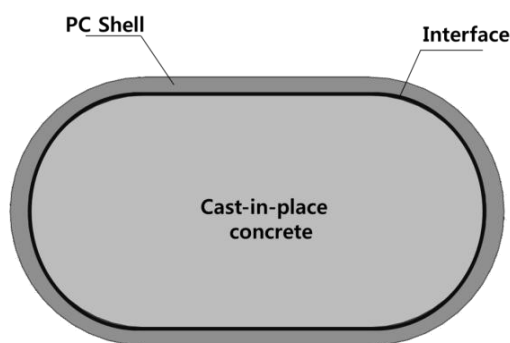


Figure 3: Interface vulnerable to cracking due to differential shrinkage

When concrete is exposed to air of lower relative humidity, the interior moisture of the concrete moves toward the surface; its distribution is highly nonlinear, following diffusion theory. As drying proceeds, the region near the surface shrinks faster than the inner area that is still wet. Consequently, tensile stress is induced

near the surface at the beginning of drying. When the tensile stress exceeds the interfacial bond strength in a PC shell pier cap, cracks initiate at the interface. The differential drying shrinkage, based on the nonlinear moisture diffusion, should be considered in predicting this cracking. Stresses due to internal or external restraints induce creep deformation, which may delay the cracking time considerably. Concrete creep should be considered together with differential drying shrinkage in the prediction of the interfacial cracking.

There is a plan to apply a PC shell pier cap to a real construction site located in Seoul, South Korea. The objective of this study is to establish a prediction method for the interfacial cracking of the PC shell pier cap that will consider the real mechanism of drying shrinkage and creep. To minimize uncertainty regarding the properties of concrete, experiments for the strength, elastic modulus, drying shrinkage, and creep were performed with the concrete mix that is supposed to be applied to manufacturing pier caps. The main material parameters used in the analysis were determined from experiments. The variation of internal relative humidity over time was first calculated based on the nonlinear moisture diffusion; cracking analysis then followed, considering the differential drying shrinkage and creep. In addition, an analysis for the case in which supplementary reinforcements are placed at the interface to reduce crack width was performed, and the effect of the reinforcement was also investigated.

2 Material models for differential drying shrinkages

2.1 Moisture diffusion and drying shrinkage

The governing equation of moisture diffusion inside concrete is expressed as follows [Bazant and Najjar (1972)]:

$$\frac{\partial h}{\partial t} = \text{div}(D \text{grad } h) \quad (1)$$

where h is the pore relative humidity, t is time, and D is the moisture diffusion coefficient. CEB-FIP MC 90 (1993) suggested the coefficient D for isothermal condition as a function of the pore relative humidity, as follows:

$$D(h) = D_1 \left(\alpha + \frac{1 - \alpha}{1 + [(1 - h)/(1 - h_c)]^n} \right) \quad (2)$$

where D_1 is the maximum of $D(h)$ for $h = 1.0$, $\alpha g = D_0/D_1$, D_0 is the minimum of $D(h)$ for $h = 0.0$, h_c is the pore relative humidity at $D(h) = 0.5D_1$, and n is an exponent. In this study, $\alpha g = 0.05$, $h_c = 0.8$, and $n = 15$ are fixed as suggested in

CEB-FIP MC 90 (1993). At the exposure surface S , the boundary condition can be expressed by the following equation [Kim and Lee (1998)]:

$$D \left(\frac{\partial h}{\partial n} \right)_s = f(h_{en} - h_s) \quad (3)$$

where f is the surface factor, h_{en} is the environmental humidity factor, and h_s is the relative humidity at the surface. The solution of Eq. (1) can be obtained from numerical analysis methods such as finite element or finite difference methods [Kwon and Shah (2008); Kwon, Ferron, Akkaya and Shah (2007); Bazant and Najjar (1972)]. Based on the analysis results for the moisture loss over time caused by drying, shrinkage strain can be calculated using the following equation [Bazant and Xi (1994)]:

$$\Delta \varepsilon_{sh} = k_{sh} \Delta H, k_{sh} = \varepsilon_s^0 g_s(t) = \varepsilon_s^0 \frac{E(t_0)}{E(t)} \quad (4)$$

where $\Delta \varepsilon_{sh}$ is the shrinkage strain increment due to the loss of the relative humidity, ε_s^0 is a material constant representing the magnitude of the final shrinkage strain at infinite time, and $E(t_0)$ and $E(t)$ are elastic modulus at times t_0 and t , respectively. Concrete shrinks faster at the region near the surface because the moisture loss is much larger near the surface at the beginning of drying. Tensile stress is induced at the part close to the surface, and the interior part is under compression to balance the difference between the shrinkage strains of the interior part and the part near the surface.

2.2 Basic creep and drying creep

The stresses caused by internal and external restraints induce creep deformation. Creep deformation can be divided into two parts: basic creep and drying creep. The former is creep deformation under non-drying conditions and can be explained using solidification theory [Bazant and Baweja (1995)]. In this study, the ACI model 209 (2000) is used as a basic creep model and is expressed as follows:

$$J(t, t') = \frac{1}{E(t')} \left(1 + \phi_u(t') \frac{(t - t')^n}{A + (t - t')^n} \right), \quad \phi_u(t') = B \times (t')^\alpha \quad (5)$$

where t' is the time at loading, t is an arbitrary time after loading, $J(t, t')$ is a compliance function including basic creep strain, $E(t')$ is an elastic modulus at time t' , $\phi_u(t')$ is the ultimate creep coefficient representing the final creep coefficient at infinite time, and A , B , α , and n are the empirical constants.

Drying creep, also known as the Pickett effect [Pickett (1942)], refers to the excess of creep at drying over the sum of the shrinkage and basic creep. This phenomenon

was recently explained in terms of stress-induced shrinkage [Bazant and Xi (1994)] based on micro-diffusion between micro pores and macro pores. Stress-induced shrinkage means that drying shrinkage strain is increased when stress is applied to concrete. Eq. (4) is changed to consider the stress-induced shrinkage strain, as follows:

$$\Delta \varepsilon_{sh,ij} = k_{ij} \Delta H, \quad k_{ij} = k_{sh} \left[\delta_{ij} + (\gamma \sigma'_{ij} + \gamma' \sigma_v \delta_{ij}) \frac{\Delta H}{\sqrt{(\Delta H)^2}} \right] \quad (6)$$

where the subscripts i and j indicate the directions of the strain and stress, respectively, δ_{ij} is the Kronecker delta, and γ and γ' are constants for the stress-induced shrinkage. In this study, the volumetric and deviatoric drying creep are assumed to be identical, that is, $\gamma = \gamma'$. In predicting the cracking, creep deformation should be considered because it may considerably delay cracking time. The stress caused by the restraints is relaxed to some extent by creep deformation, and cracks initiate when the resultant stress reaches the tensile strength of the concrete.

In Eq. (5), the elastic modulus of concrete at an arbitrary time is needed, and the following equation [CEB-FIP MC 90 (1993)] is used to fit the measured elastic modulus at different ages.

$$E(t) = E(28) \sqrt{\exp \left[\beta \left(1 - \frac{28}{t} \right)^\eta \right]} \quad (7)$$

Here, $E(t)$ is the elastic modulus at time t , $E(28)$ is the elastic modulus at 28 days, and β and η are empirical constants.

2.3 Behavior at the interface between precast and cast-in-place concrete

The behavior at the interface between the outer precast shell and the inner cast-in-place concrete can be expressed using the Coulomb friction model, as follows [Kwon, Kim and Kim (2005)]:

$$\tau_{crit} = \mu p + c \quad (8)$$

where τ_{crit} is the friction stress or the shear strength, μ is the friction coefficient, p is the compressive stress in the direction normal to the interface, and c is the cohesion. If the shear stress exceeds the friction stress, slip at the interface would occur. In a case in which the normal stress is tension and exceeds the cohesion, it was assumed that brittle gapping at the interface would occur.

3 Experiments for determination of material parameters

3.1 Test program

Figure 4 shows the dimensions of the PC shell pier cap that will be applied to a real construction site located in Seoul, South Korea. The precast outer shell and the inner body will be manufactured with the same concrete, of which the mix proportion is listed in Table 1. The specified strength of the mix was 40 MPa. Cylinder specimens of $\phi 150 \times 300$ mm were manufactured and cured at 100% relative humidity (RH) until shortly before testing. Table 2 provides the test program. The compressive strength and the elastic modulus were measured at the ages of 2, 7, 14, and 28 days. Concrete embedment gages were installed in the middle of the specimens to measure the variations of the strains over time in the shrinkage and creep tests.

The shrinkage specimens were exposed to air of 60% RH at the ages of 3, 7, and 14 days. Creep tests were carried out in two different conditions: sealed condition and drying condition. In the former condition, the specimens were sealed with plastic film, and the basic creep was measured under a sustained load corresponding to 20% of the compressive strength at different loading ages of 3, 7, and 14 days. The creep tests were performed with the specimens exposed to air of 60% RH. The drying creep was extracted from the total strain measured in the drying condition, which include the drying shrinkage, basic creep, and drying creep. All tests were performed at a constant temperature of 23 °C; the test setups are shown in Fig. 5.

Table 1: Mix proportions

w/b (%)	S/a (%)	Unit weight (kg/m ³)							
		Water	*Binder			Sand		Gravel	****SP
			Cement	Fly-ash	BFS	**S1	***S2		
50	45	168	249	99	149	528	227	928	3.48

*BFS : blast furnace slag, **S1 : sea sand, ***S2 : crushed sand, ****SP : superplasticizer

Table 2: Test program

Compressive Strength & Elastic Modulus	Drying Shrinkage	Creep	
		Basic Creep	Drying Creep
Testing age (days)	Age at exposure (days)	Age at loading (days)	
2, 7, 14, 28	3, 7, 14	3, 7, 14	

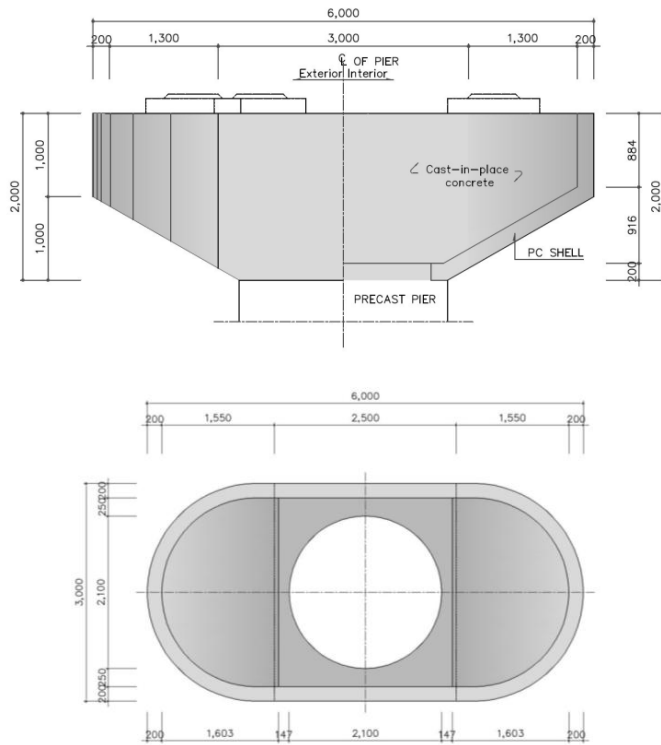


Figure 4: Dimensions of precast shell pier-cap



(a) Strength and elastic modulus



(b) Drying shrinkage



(c) Creep

Figure 5: Tests for concrete used in the precast shell pier-cap

3.2 Determination of materials parameters from test results

The measured compressive strengths and elastic moduli are plotted over ages in Fig. 6. The actual strength at 28 days was 46.6 MPa, more than the specified strength. The parameters, β and η , of Eq. (7) were determined by curve fitting the measured elastic moduli as 0.117 and 0.857, respectively. The curve fit result is also displayed in Fig. 6.

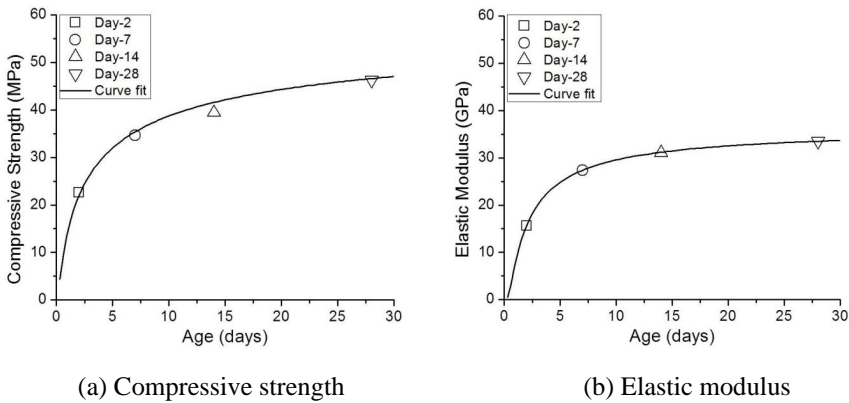


Figure 6: Test and curve fit results for compressive strength and elastic modulus

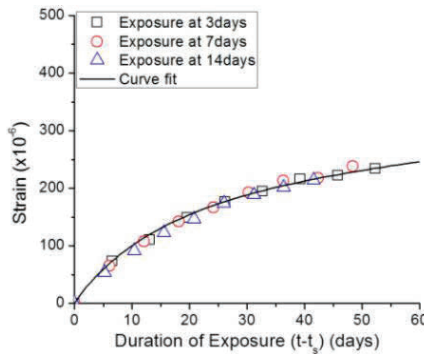


Figure 7: Test and curve fit results for drying shrinkage

Figure 7 shows the results of the drying shrinkage tests. It does not seem that the shrinkage strain depends on the age during exposure to air of lower relative humidity. By repeating numerical analyses for the differential drying shrinkage

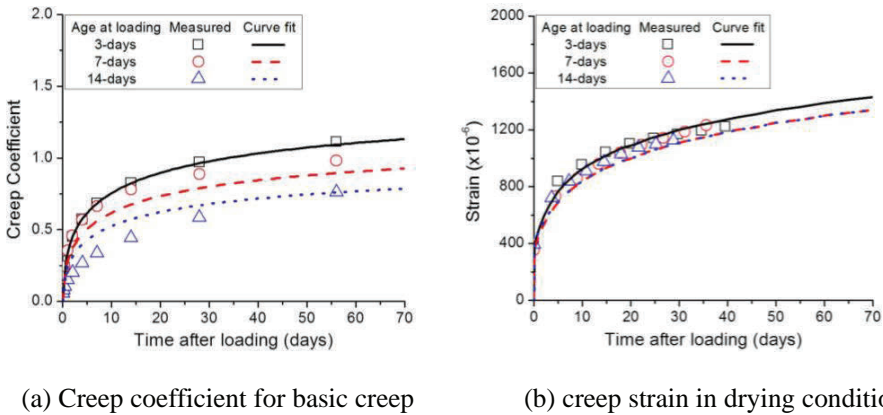


Figure 8: Test and curve fit results for creep

Table 3: Parameters determined from tests

Tests	Determined Parameters
Elastic modulus Eq.(7)	$\beta = 0.177$ $\eta = 0.857$ $E(28) = 33.5 \text{ MPa (measured)}$
Moisture diffusion Eqs. (2), (3) and (4)	$D_1 = 18.0 \text{ (mm}^2\text{/day)}$ $f = 1.0 \text{ (mm/day)}$ $\epsilon_s^0 = 13 \times 10^{-6}$
Basic creep Eq. (5)	$n = 0.153$ $A = 3.61$ $B = 2.06$ $\alpha = - 0.236$
Drying creep Eq. (6)	$\gamma = g\gamma' = 0.007$

of the specimens based on the moisture diffusion, the parameters D_1 , f , and ϵ_s^0 , of Eqs. (2), (3), and (4), optimally fitting the measured shrinkage strains, were determined and are listed in Table 3. The curve fit results show a good agreement with the measured results.

The creep coefficient is defined as the ratio of the creep strain to the elastic strain. The strains measured from the basic creep tests were transformed into creep coefficients; these are plotted over age in Fig. 8(a). The creep coefficient depends on the age at loading. The parameters, A , B , α , and n of Eq. (5) were determined by curve fitting the creep coefficient transformed from the basic creep test results; the

determined parameters are also listed in Table 3.

When the specimen was subjected to a sustained load under drying condition, the measured strains include the drying shrinkage, basic creep, and drying creep. The shrinkage strains shown in Fig. 7 and the basic creep strains shown in Fig. 8(a) were subtracted from the total strains to obtain drying creep strains. The parameter, γ , of Eq. (6) was determined by fitting the drying creep strains as 0.007. Fig. 8(b) shows the creep strains measured in the drying condition and the curve fit results.

4 Finite element analysis for precast pier cap

4.1 General

Finite element modeling was conducted for the PC shell pier cap illustrated in Fig. 4. Considering the symmetry of the pier cap, one fourth of the pier cap was modelled as shown in Fig. 9. The outer precast shell and the inner concrete were considered as separate bodies in the process of modeling, the interface element was inserted between the bodies. The reinforcements inside the concrete were also realistically modelled with the embedded elements. Nonlinear moisture diffusion analysis was first performed, and then shrinkage strain, creep, and cracking were calculated based on the time-varying internal moisture distribution, obtained from the moisture diffusion analysis. A commercial computer program was used in the finite element analysis. The material models used in this study are not provided by the program, and a specially coded subroutine for the models was incorporated into the program.

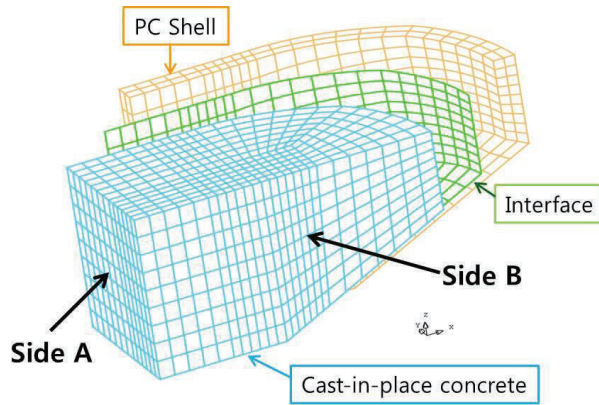
4.2 Modeling

A solid element with 20 nodes was used to model the outer shell and the inner concrete. The numbers of elements for the outer shell, the inner concrete, and the interface were 984, 2484, and 492, respectively.

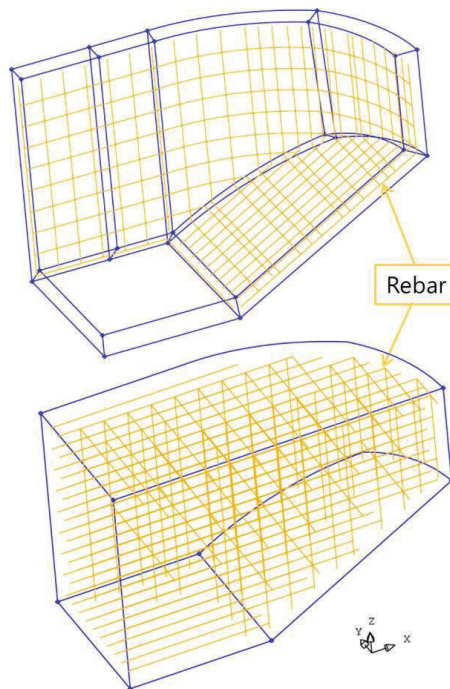
Interfacial cracking was simulated with the model described in subsection 2.3. Based on the existing study, the friction coefficient μ and the cohesion c in Eq. (8) were set to 0.5 and 0.5MPa, respectively.

The parameters of the material models for the moisture diffusion, the shrinkage, and the creep of concrete were determined as explained in subsection 3.2 and are summarized in Table 3. These parameters were used in the analysis. The elastic modulus of the reinforcements was 200 GPa; the Poisson's ratio of the concrete was 0.2.

In the analysis, the actual construction schedule of the pier cap was considered, as follows. The outer shell was cured for 7 days and remained open to air of 60%



(a) Mesh refinement for separate bodies



(b) Reinforcements embedded inside the bodies

Figure 9: Finite element modeling for precast shell pier-cap

RH for 28 days after curing. The next step was to pour concrete inside the shell. The inner concrete was cured for 7 days and then exposed to air of 60% RH. The material properties of concrete, depending on the age, were also taken into account in the analysis.

4.3 Modeling additional reinforcements across the interface

As a countermeasure to reduce the interfacial cracking, reinforcement across the interface can additionally be placed. The reinforcement strengthens the bond strength of the interface in the tensile direction, in addition to the cohesion of Eq. (8). CEB-FIP MC 90 (1993) gives the bond-slip relationship for embedded rebar; this relationship can be easily transformed into the relationship between the tensile stress over the interface and the crack opening. Figure 10 shows a typical bond stress-slip relationship.

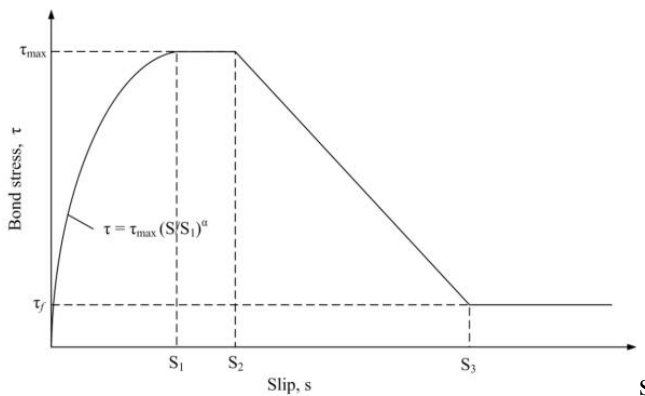


Figure 10: Bond stress-slip relationship for rebar

The value of $\tau_{\tau_{max}}$ is transformed into the maximum tensile stress, as follows:

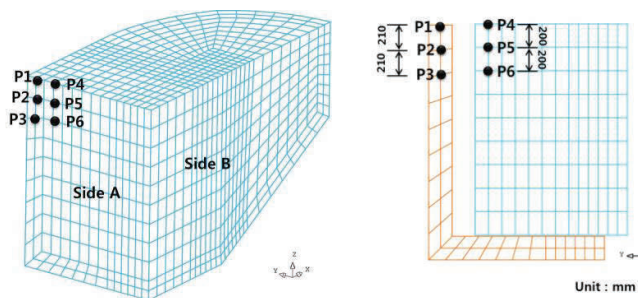
$$\sigma_{t,max} = \frac{\tau_{max} \times (\pi D_s) \times l}{A_e} \tag{9}$$

where $\sigma_{t,max}$ is the transformed maximum tensile stress over the interface, $\tau_{\tau_{max}}$ is given by the CEB-FIP MC 90 (1993), D_s is the nominal diameter of the rebar, l is the embedded length of the rebar, and A_e is the cross-sectional area of the interface element across which the rebar is placed. The slips S_1 , S_2 , and S_3 , which can be considered as crack openings at the interface, are also specified in the CEB-FIP MC 90 (1993).

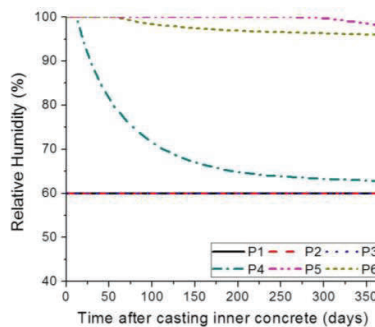
5 Results and discussion

5.1 Relative humidity distribution

Moisture diffusion analysis was first performed for one year after casting the inner concrete. In Fig. 11, the relative humidity at different positions is plotted over time. Because the outer shell remained open to the air for a long time before casting of the inner concrete, and because the shell thickness is very thin, the internal humidity of the shell had already reached the external relative humidity of the air. On the other hand, the moisture of the inner concrete mainly evaporated near the top surface for one year. The relative humidity at the surface (P4) was found to decrease over time and reached an almost constant value one year after exposure. At position P5, which is 200 mm away from the top surface, the concrete was still wet, with more than 95% RH, even one year after exposure.



(a) Distribution of relative humidity inside the pier cap at 28 days after casting the inner concrete



(b) Variation of internal relative humidity over time at different positions

Figure 11: Results for the moisture diffusion analysis

The variation of the relative humidity near the surface of the inner concrete may cause the interfacial cracking. Based on the results of moisture diffusion analysis, cracking analysis was performed considering the shrinkage and the creep.

5.2 Cracking

Figure 12 shows the deformed shape and the cracking at the top surface, which is 300 times magnified than the calculated deformations. It can be seen that cracks occur at the top surface of the pier cap in two square planes of symmetry, at Position 1 and Position 2. The maximum cracking widths at Position 1 and Position 2 were plotted over time with the solid lines shown in Fig. 13. The crack widths increased with the increase of time and exceeded 0.3 mm at around 150 days. After 150 days, the crack width remained almost constant at Position 1, whereas the width at Position 2 kept increasing over time. For reasons of serviceability and durability, crack width larger than 0.3 mm is generally not allowed in the design codes, and a method is needed to reduce crack width.

As mentioned above, an analysis of cases in which supplementary reinforcements are placed at Position 1 and Position 2 was performed and the effect of such reinforcement was also investigated.

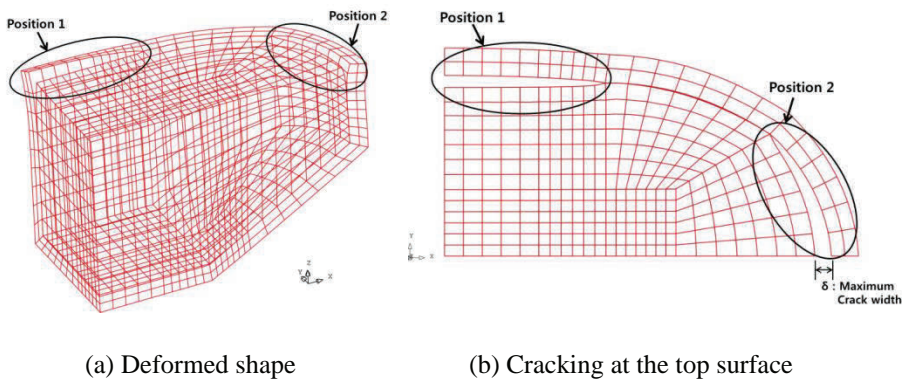


Figure 12: Deformed shape and cracking at the top surface of the pier cap without interfacial reinforcement

5.3 Effect of interfacial reinforcement on cracking

In this study, an analysis of cases in which supplementary reinforcements were placed across the interface was performed, with results as shown in Fig. 14. Two pieces of rebar with nominal diameter of 15.9 mm and embedded length of 200 mm

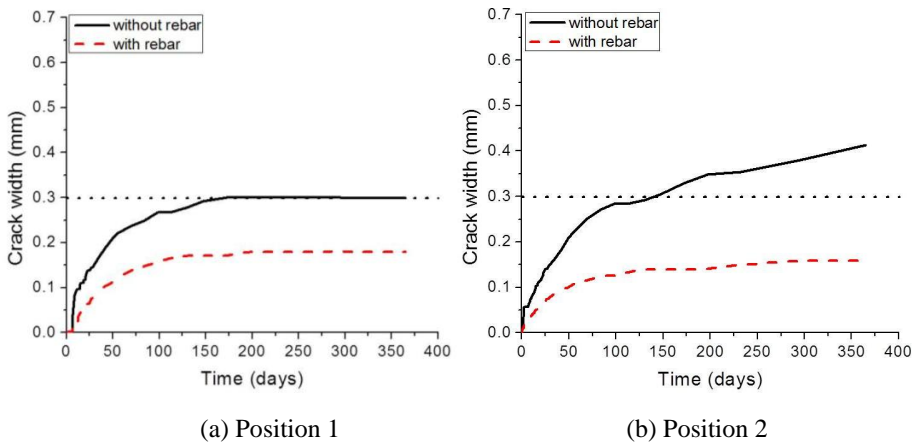


Figure 13: Variation of crack width over time

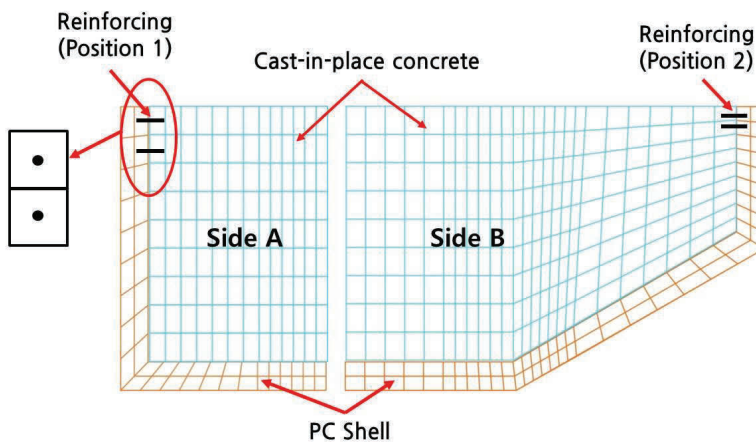


Figure 14: Reinforcements to strengthen interfacial bonds at critical regions

were assumed to have been installed 100 mm away from the top surface of the pier cap in the two square planes of symmetry. The cross sectional area, A_e , from Eq. (9), was 28,000 mm². Referring to the CEB-FIP MC 90 (1993), the parameters, S_1 , S_2 , and S_3 were set at 0.6, 0.6, and 1.0 mm, respectively.

Figure 15 shows the deformed shape and the cracking at the top surface of the pier cap with interfacial reinforcement. Differently from the case in which no interfacial reinforcement was used, as shown in Fig. 12, the crack was almost closed at the location at which the rebar was placed. The maximum crack widths at Position 1

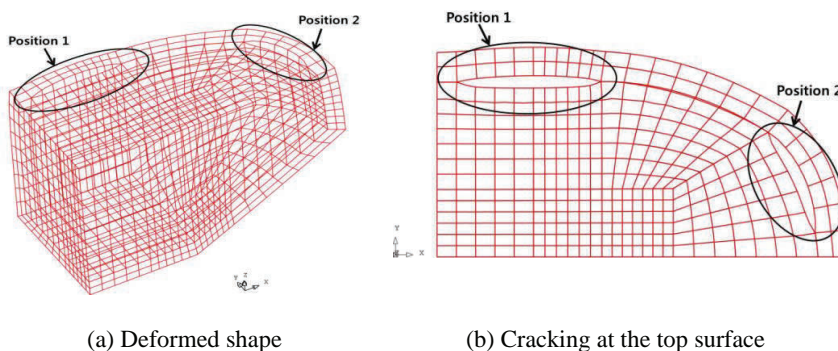


Figure 15: Deformed shape and cracking at the top surface of the pier cap with interfacial reinforcement

Table 4: Maximum crack width

Interface conditions	Crack Width (mm)	
	Position 1	Position 2
No reinforcement	0.30	0.41
Reinforcement	0.18	0.16

and Position 2 are also plotted over time in Fig. 13. It can be seen that the crack width was greatly reduced and did not exceed 0.3 mm. The maximum crack widths in all of the analysis cases are listed in Table 4. The interfacial reinforcement reduced the crack widths at Position 1 and Position 2 by as much as 40% and 60%, respectively.

6 Conclusions

In a precast shell pier cap, cracking at the interface between the precast shell and the cast-in-place concrete may be induced due to differences between the drying shrinkage of the inner and the outer concrete. From the aspects of durability and serviceability, crack width should be less than a certain value specified in the design code. Therefore, it is necessary to estimate the interfacial cracking in the process of design and construction.

Through this study, a method to predict interfacial cracking in precast shell pier caps was established. The actual mechanism for the interfacial cracking, as well as the construction schedule, were taken into account in the analysis. To minimize uncertainty of the concrete properties, the main parameters used in the analysis were

determined by experiments with the same concrete mixture applied to the construction of pier caps. Based on nonlinear moisture diffusion analysis, the variation of the internal relative humidity over time was first calculated; cracking analysis then followed. The initiation of interfacial cracks and the increase of their width over time were predicted using the established analysis method. It was also found that additional reinforcement across the interface is very effective at reducing the crack width. In the near future, although it is necessary to verify that predictions for interfacial cracking can yield good agreement with actual cracking behavior, it is expected that the methodology suggested in this study can be applied to predicting of interfacial cracking not only for precast pier caps but also for other members that have interfaces between two concrete surfaces cast at different ages.

Acknowledgement: This work was financially supported by the Samsung C&T Corporation. The first author is very grateful for the support.

References

ACI Committee 209. (2000): *Prediction of Creep, Shrinkage, and Temperature Effects in Concrete Structures*. American Concrete Institute, Detroit, MI, USA, ACI 209 R-92

Bazant, Z. P.; Xi, Y. (1994): Drying Creep of Concrete: Constitutive Model and New Experiments Separating its Mechanisms. *Materials and Structures*, vol. 27, no. 1, pp. 3-14.

Bazant, Z. P.; Baweja, S. (1995): Creep and Shrinkage Prediction Model for Analysis and Design of Concrete Structures-Model B3. *Materials and Structures*, vol. 28, pp. 357-365

Bazant, Z. P.; Najjar, L. J. (1972): Nonlinear Water Diffusion in Nonsaturated Concrete. *Materials and Structures*, vol. 5, no. 25, pp. 3-20.

Chung, C. H.; Lee, J.; Gil, J. H. (2013): Structural Performance Evaluation of a Precast Prefabricated Bridge Column under Vehicle Impact Loading. *Structure and Infrastructure Engineering*, pp. 1-15.

Comite Euro-International Du Beton (1993): CEB-FIP Model Code 1990 *Thomas Telford*.

G. Pickett (1942): The Effect of Change in Moisture Content on the Creep of Concrete under a Sustained Load. *ACI Journal*, vol. 38, pp. 333-355.

Kim, T. H.; Lee, H. M.; Kim, Y. J.; Shin, H. M. (2010): Performance Assessment of Precast Concrete Segmental Bridge Columns with a Shear Resistant Connecting Structure. *Engineering Structures*, vol. 32, pp. 1292-1303.

Kim, J. K.; Lee, C. S. (1998): Prediction of Differential Drying Shrinkage in Concrete. *Cement and Concrete Research*, vol. 28, no. 7, pp. 985-994.

Kwon, S. H.; Shah, S. P. (2008): Prediction of Early-Age Cracking of Fiber-Reinforced Concrete due to Restrained Shrinkage. *ACI Materials Journal*, vol. 105, no. 4, pp. 381-389.

Kwon, S. H.; Ferron, R. P.; Akkaya, Y.; Shah, S. P. (2007): Cracking of Fiber-Reinforced Self-Consolidating Concrete due to Restrained Shrinkage. *International Journal of Concrete Structures and Materials*, vol. 1, no. 1, pp. 3-9.

Kwon, S. H.; Kim, Y. Y.; Kim, J. K. (2005): Long-term Behaviour under Axial Service Loads of Circular Columns made from Concrete Filled Steel Tubes. *Magazine of Concrete Research*, vol. 57, no. 2, pp. 87-99.

Lee, J. H.; Son, J. K.; Yoo, D. H.; Shin, S. J. (2010): Optimum Design and Accelerated Construction of Bridge Pier Cap. *Magazine of Korea Concrete Institute*, vol. 22, no. 6, pp. 71-76.

Park, B. S.; Park, S. H.; Cho, J. Y. (2013): A Pre-assembly Method of Steel Reinforcement to Improve the Constructability of Pier Coping. *Engineering Structures*, vol. 48, pp. 166-175.

Shim, C. S.; Chung, C. H.; Kim, H. H. (2008): Experimental Evaluation of Seismic Performance of Precast Segmental Bridge Piers with a Circular Solid Section. *Engineering Structures*, vol. 30, pp. 3782-3792.

